Control-Structure Interaction in Precision Pointing Servo Loops

John T. Spanos*
Jet Propulsion Laboratory, California Institute of Technology, Pasadena, California

The control-structure interaction problem is addressed via stability analysis of a generic linear servo loop model. With the plant described by the rigid body mode and a single elastic mode, structural flexibility is categorized into one of three types: 1) appendage, 2) in-the-loop minimum phase, and 3) in-the-loop nonminimum phase. Closing the loop with proportional-derivative (PD) control action and introducing sensor roll-off dynamics in the feedback path, stability conditions are obtained. Trade studies are conducted with modal frequency, modal participation, modal damping, loop bandwidth, and sensor bandwidth treated as free parameters. Results indicate that appendage modes are most likely to produce instability if they are near the sensor rolloff, whereas in-the-loop modes are most dangerous near the loop bandwidth. The main goal of this paper is to provide a fundamental understanding of the control-structure interaction problem so that it may benefit the design of complex spacecraft and pointing system servo loops. In this framework, the JPL Pathfinder gimbal pointer is considered as an example.

Introduction

THE control-structure interaction problem in large space vehicles is one of the most difficult and interesting problems that the aerospace community has had to contend with in recent years. While control system performance requirements are being pushed upward, today's spacecraft are built lighter and more flexible than ever before. Consequently, this trend tends to increase the potential for strong interactions between the vehicle structure and its onboard controller. Thus, structural flexibility is one of the major considerations in the design, analysis, and simulation of spacecraft pointing servo loops.

High control system performance is realized via high loop bandwidth, which in turn is limited by structural flexibility and hardware dynamics (i.e., actuator and sensor rolloff and noise characteristics). High bandwidth translates into high speed of response, good disturbance rejection, and good steady-state tracking. In single-input/single-output (SISO) position controlled systems, high loop bandwidth is typically achieved via PD control action, although for rate controlled systems proportional-integral (PI) control is often used. These types of low-order compensators find wide use in practice, primarily due to their simplicity and good robustness properties with respect to plant variations.

Another favorable property of PD control on position (or PI on rate) is that it will not destabilize a structure dominated by appendage flexibility. Appendage-type flexibility is characteristic of spacecraft solar panels (Fig. 1) and it is mathematically described by sequentially alternating poles and zeros in the plant transfer function.[1,2] Root locus analysis has shown that the PD zero draws the undamped closed-loop poles into the left half of the complex plane along a stable path.[1,2] This property of stable control-structure interaction makes PD control a leading candidate for stabilization of appendage flexibility. However, the PD and plant dynamics are almost never alone in a servo loop. Low frequency dynamics in the feedback path are usually present in the form of 1) sensor roll-off dynamics, 2) low-pass filter dynamics used to remove sensor noise that would otherwise pass through to the output, and 3) anti-aliasing filter dynamics guarding against higher mode aliasing in digital computer implementations.

Received Aug. 21, 1987; revision received Jan. 4, 1988.

*Member, Technical Staff, Guidance and Control Section.

Consequently, appendage flexibility under PD control can be driven unstable. Considering that the controller gains and, hence, loop bandwidth are first designed on the basis of rigid body plant assumptions, it is desirable to know the amount, type, and frequency content of flexibility that could lead to marginal stability in the system. Thus, there is a limit to how much the servo loop gain can be raised before the control-structure interaction becomes severe enough to destabilize the system.

The interaction problem between appendage flexibility and the various control system components has received attention by the practicing community. Designers of reaction jet attitude control systems have studied the strong interactions between solar array flexibility and nonlinear elements such as pulse width, pulse frequency modulators. Utilizing describing function techniques, nonlinear stability margins guarding against the limit cycle condition of the appendage mode were determined.[3] Further work in the area of active vibration suppression via collocated direct velocity feedback has addressed the issue of stability in the presence of finite actuator bandwidth. Perturbation methods were used to decouple a high-order structural model to its many modal subsystems, and stability analysis was carried out on a per-mode basis. It was demonstrated that collocated control using velocity feedback will have a destabilizing effect on the high-frequency modes when the second-order low-pass actuator dynamics are modeled.[4]

When the actuator and sensor are placed next to each other on the structure (i.e., collocated control), appendage flexibility is the only possible type present in the servo loop. Although this is the most common type encountered in large space structures, it is not the only type. Collocated control is not always possible, and recent dual-spinner spacecraft such as Galileo[5] and OSO-8[6] (Orbiting Solar Observatory-8) have reported noncollocated control with significant in-the-loop structural flexibility. Simple experiments conducted on torsional disk systems with in-the-loop type flexibility have indicated that noncollocated control is a great threat to servo loop stability.[7] Yet, control systems with noncollocated actuators and sensors continue to be planned for future planetary spacecraft. Attitude control of the three-axis stabilized Mariner Mark II spacecraft (currently in the conceptual design phase) is to be provided by servoing the propulsion thrust vector via a gyro sensor mounted at the end of a flexible boom.[8]

Through the years it has become common knowledge that in order to avoid potential control system instability, the designer

must avoid placing the open-loop crossover frequency close to a frequency of a major structural mode. A conservative approach to control system design for the purposes of avoiding control-structure interaction has been to keep the loop bandwidth an order of magnitude smaller than the first structural mode. This action often results in gain stabilization by loop roll-off. For high performance systems exhibiting severe control-structure interactions, classical gain and phase stabilization by means of appropriate filtering (i.e., notch filtering) has been used extensively.[2,3,5,6,9]

The purpose of this paper is to provide a fundamental understanding of the control-structure interaction in a high gain servo loop by exploiting the stability viewpoint. Finite-element modeling of structures is briefly reviewed for the purposes of obtaining a detailed multimode model of the plant under control. In order to understand the nature of the control-structure interaction problem, stability analysis of a linear sixth-order servo loop model is proposed. The loop components are 1) a fourth-order plant model described by the rigid-body mode and a single flexible mode, 2) a second-order low-pass model describing the roll-off dynamics in the feedback path, and 3) the PD controller dynamics.

Based on structural mode pole-zero patterns, flexible modes are categorized into one of three types: 1) appendage, 2) in-the-loop minimum phase, and 3) in-the-loop nonminimum phase. Stability analysis of the idealized sixth-order linear servo loop model is carried out, and closed-form stability conditions directed toward each of the three flexibility types are obtained. Trade studies are carried out among the system parameters, and single-mode and multi-mode examples (among them the JPL Pathfinder gimbal) are presented. Results indicate that the second-order low-pass dynamics have a stabilizing effect on the in-the-loop modes, but a destabilizing effect on the appendage modes.

Finite-Element Modeling

Dynamic modeling of complex structural systems is typically accomplished via the finite-element method. The structure is discretized into a large number of nodes each of which is generally allowed 6 degree-of-freedom (DOF) motion. For a single actuator (input) located at nodal DOF i, and single sensor (output) located at nodal DOF j, the system dynamics are commonly described by the transfer function relation[1]

$$\frac{x_j(s)}{f_i(s)} = \frac{1}{Js^2} + \sum_{k=R+1}^{m} \frac{\phi_{ik}\phi_{jk}}{s^2 + 2\zeta\omega_k s + \omega_k^2} \tag{1}$$

where x_j, f_i are the nodal displacements and forces, respectively, the pair $\{\omega_k, \phi_{jk}\}$ represents the m natural frequencies and corresponding mode shapes of vibration (normalized to unit mass), ζ is the damping rate (typically 0.1–1% of critical), and J is the effective rigid-body inertia of a plant with R rigid-body modes. The effective rigid-body inertia can be obtained in terms of the mode shapes as follows:

$$J = \frac{1}{\sum_{k=1}^{R} \phi_{ik}\phi_{jk}}$$

Equation (1) represents an exact residues model of the SISO plant. Methods for obtaining an exact pole-zero model are available[10] but will not be discussed herein. It should be emphasized that the model of Eq. (1) forms the basis upon which compensator design, loop stability, small motion simulation, and "first cut" performance assessment are accomplished.

Single Mode Model

Definition and Justification

The pointing and tracking control problem in large space structures would be much easier if the structure behaved like a rigid body. It is the inherent coupling between the rigid and flexible modes that causes most of the stability and performance related problems that are encountered today. The control effort applied to point the "rigid body" excites the flexible modes, which can destabilize the system or cause enough ringing to prevent meeting pointing stability (i.e., jitter) requirements. (In the large space structures community this is known as the control spillover problem.[11])

In view of this discussion, the simplest of models capable of capturing the rigid and flexible dynamics interaction to the first order is one consisting of a single rigid and a single flexible mode. This type of model has received a lot of attention in the literature, although different authors have used it to make different points.[3,4,9,10,12–15] Yet, the single mode model has not been formally defined to accommodate all possible types of structural flexibility, nor has it been made clear how the results so obtained extrapolate to the more realistic multimode model. In an effort to establish a link with the multimode model, the proposed plant model will be extracted from Eq. (1) by retaining a single flexible mode along with the rigid-body mode. Retaining the kth flexible mode one obtains

$$\frac{x_j(s)}{f_i(s)} = \frac{1}{Js^2} + \frac{\phi_{ik}\phi_{jk}}{s^2 + 2\zeta\omega_k s + \omega_k^2} \tag{2}$$

Putting Eq. (2) under a common denominator yields

$$\frac{x_j(s)}{f_i(s)} = \frac{1}{J}\frac{\alpha_k s^2 + 2\zeta\omega_k s + \omega_k^2}{s^2(s^2 + 2\zeta\omega_k s + \omega_k^2)} \tag{3}$$

where α_k is the modal participation coefficient of mode k defined by

$$\alpha_k \equiv 1 + J\phi_{ik}\phi_{jk} \tag{4}$$

If the kth mode is minimum phase it can be easily shown that

$$\alpha_k = \omega_k^2/\Omega_k^2 \tag{5}$$

where Ω_k is the zero frequency of the single mode plant. Here it should also be made clear that Ω_k is not necessarily equal to the corresponding kth exact zero frequency of the multimode model. If one's motive is to approximate a multimode model via a single mode model at a particular frequency range of interest, and Ω_k is much different from the exact zero, then the value of α_k should be computed from Eq. (5), with Ω_k replaced by the exact zero. Obviously, this can be done only if the exact zero frequency is known and can be associated to the corresponding pole frequency.

On this note, the task of handling the multimode model reduces to pairing up the rigid-body mode with each of the flexible modes one at a time and analyzing the resulting fourth-order subsystems one at a time. This approach is justifiable as long as damping is small and structural modes are sufficiently separated in frequency. Of course, better damped systems or systems with many closely spaced modes may or may not render themselves to such a simple treatment.

The advantage in having the model casted in the form of Eqs. (3–5) is that one could easily take either modal data $(\omega_k, \phi_{ik}, \phi_{jk})$ from an output of a finite-element program (i.e., NASTRAN) or look up resonance-antiresonance frequencies (ω_k, Ω_k) from an experimentally or analytically obtained frequency response plot (i.e., Bode plot) and construct a single mode equivalent plant model. Another use is in the preliminary assessment of structural flexibility while designs are still in their feasibility stage and detailed finite-element models such as that of Eq. (1) have yet to be created. In this regard, control engineers often think of the anticipated fundamental frequency of a structure as an indication of how flexible it will be and subsequently how difficult the control-structure interaction problem will be. Single mode models with first cut control laws can be used to address the severity of the control-structure interaction

problem at a preliminary level by performing trades on the design parameters of interest.

Characterization of Structural Flexibility

Because structures under collocated control are characterized by the unique alternating pole-zero pattern,[1,2] and more importantly since the poles and zeros of the plant are always key items of interest to the controls engineer, it makes sense to classify the flexible mode of the single mode plant in terms of its pole-zero pattern. Pole-zero maps for single mode spring-mass systems have been studied as a function of sensor location.[14] Here, similar pole-zero maps will be used to categorize the modes.

Assuming that the damping is the same in every mode, another look at the model of Eq. (3) reveals that the flexible mode is identified by only two parameters: first, the modal resonance frequency ω_k, and second, the modal participation coefficient α_k or equivalently the modal antiresonance frequency Ω_k. Ignoring the damping altogether, fixing ω_k on the imaginary axis and adding the rigid-body double pole at zero, one obtains the s-plane pole patterns shown in Fig. 2. In the absence of damping, the zero Ω_k can be 1) on the imaginary axis and between the rigid and flexible poles (Fig. 2a), 2) on the imaginary axis and higher than the flexible pole (Fig. 2b), or 3) on the real axis and symmetrically spaced about the origin (Fig. 2c). Certainly the location of the modal zero with respect to its pole is of extreme importance as it affects the control problem differently. Thus, there is a need to type these patterns so that control system stability with respect to each can be studied systematically. One will note that all three of the pole-zero patterns can be identified by a single parameter: the modal participation coefficient α_k. In view of this observation, the following definitions are introduced.

1) An *appendage* mode is one whose zero lies on the imaginary axis of the s-plane and is smaller than its pole, or simply $\alpha_k > 1$.

2) An *in-the-loop minimum phase* mode is one whose zero lies on the imaginary axis of the s-plane and is larger than its pole, or simply $0 < \alpha_k < 1$.

3) An *in-the-loop nonminimum phase* mode is that which has a zero on the right half of the s-plane, or simply $\alpha_k < 0$.

From the frequency response viewpoint, the following interpretation can be given. For an appendage mode, the antiresonance will occur first contributing phase to the plant (up to 180 deg), whereas the resonance that follows will take away the same amount. For an in-the-loop minimum phase mode, the exact opposite is true. However, an in-the-loop nonminimum phase mode will not exhibit an antiresonance, and the plant will always end up losing 180 deg of phase after the resonance. This is why nonminimum phase modes are most dangerous to control system stability.

Examples of the three modal types can be given in terms of simple spring-mass models. The case of appendage flexibility is clearly illustrated in Fig. 3a where both actuator and sensor are collocated on the bus J_1. The case of in-the-loop minimum phase flexibility could also be produced by the model of Fig. 3a with the actuator on the bus, but with the sensor measuring a linear combination of the bus and appendage motion [i.e., output: $\theta = (1 - C)\theta_1 + C\theta_2$; $C > J_2/(J_1 + J_2)$].[14] Finally, the simplest example of in-the-loop nonminimum phase flexibility is the single mode spring-mass representation of a flexible beam with actuator and sensor located at opposite ends (Fig. 3b).

From the above it is clear that appendage modes are synonymous with collocated control, but this does not necessarily imply that they will not be found in noncollocated systems. On the other hand, both types of in-the-loop modes are synonymous with noncollocated control and they do imply noncollocation. Also, note how naturally the modal participation coefficient α_k divides the three modal types. When $\alpha_k = 1$, the plant degenerates to a two-pole only rigid system. For $\alpha_k = 0$, it is a four-pole only system, and for $\alpha_k = \pm\infty$, it is a two-pole only flexible system. Thus, using the proper value of α_k in Eq. (3) allows one to synthesize a single mode plant model with the desired type of flexibility.

Mass Participation in Appendage Modes

The most common form of appendage flexibility is encountered in space vehicles with large solar panels (see Fig. 1). A one-axis discrete model often used to study attitude control/solar panel interaction is the 2-DOF torsional spring-mass system shown in Fig. 3a. The rigid central core (i.e., bus) of the spacecraft is represented by the concentrated inertia J_1, the solar panel inertia is J_2, and panel structural flexibility is modeled by the spring K. The system frequencies and mode shapes Ω, Φ can be written in terms of the physical parameters J_1, J_2, K as follows:

$$\Omega = \begin{bmatrix} 0 & 0 \\ 0 & \sqrt{\dfrac{KJ}{J_1 J_2}} \end{bmatrix}, \qquad \Phi = \begin{bmatrix} \dfrac{1}{\sqrt{J}} & \sqrt{\dfrac{J_2}{J_1 J}} \\ \dfrac{1}{\sqrt{J}} & -\sqrt{\dfrac{J_1}{J_2 J}} \end{bmatrix}$$

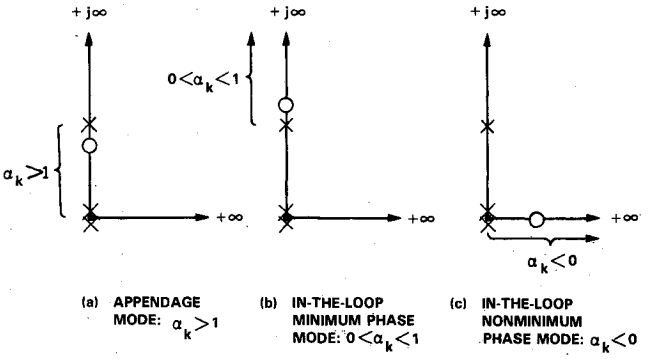

Fig. 2 Pole-zero patterns for each modal type.

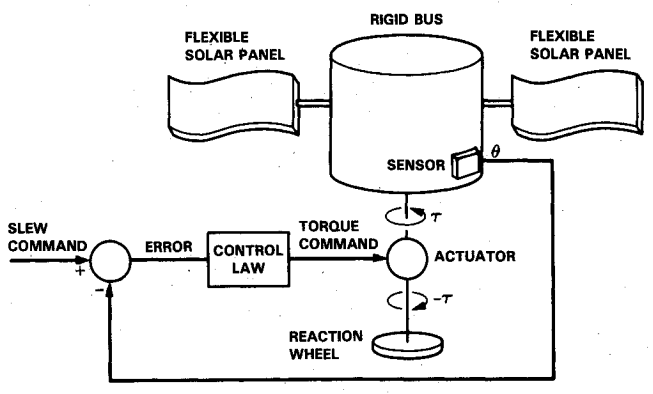

Fig. 1 Appendage-type flexibility in a momentum controlled spacecraft.

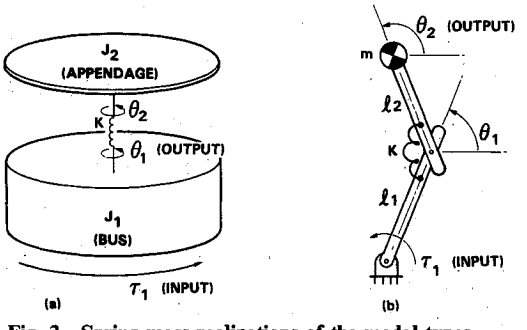

Fig. 3 Spring-mass realizations of the modal types.

when J represents the total inertia of the vehicle, or $J = J_1 + J_2$. Define the percent mass participation in the flexible mode as

$$\mu \equiv \frac{J_2}{J} \times 100\% \tag{6}$$

Intuitively, this represents the amount of mass vibrating in the flexible mode. Note that in this context the words mass and inertia are used interchangeably. Equation (6) can be written in terms of the modal data as

$$\mu = \frac{J\phi_{12}^2}{1 + J\phi_{12}^2} \times 100\% \tag{7}$$

One will recognize that the denominator of Eq. (7) is identical to the modal participation coefficient α_k as defined in Eq. (4) for $k = 2$. On this basis and whenever applicable, the concept of the percent mass participation can be extended to higher order finite-element models via the single mode equivalent model. For a plant with multiple appendage modes that may or may not be characterized by a collocated actuator-sensor pair, the percent mass participation coefficient can be expressed in terms of the modal participation coefficient α_k as follows:

$$\mu_k = \left(1 - \frac{1}{\alpha_k}\right) \times 100\% \tag{8}$$

Thus, an appendage mode can be signified by the percent mass participation μ_k, which provides the physical feel of Fig. 3a. However, it should be noted that for a multimode model, μ_k serves only as an indicator of mass participation and it is not to be confused with the true mass participating in the kth mode. (For more information on the true mass participation in multimode systems, see Bamford et al.[16])

Stability Analysis

Infinite Sensor Bandwidth

Having constructed the single mode plant model, attention is now focused on the control problem. One of the most fundamental control laws frequently considered in practice is the PD. Often, integral action (I) is used with the PD for good steady-state tracking of the reference inputs, but it will not be considered herein. The loop block diagram of Fig. 4 shows a PD controller implemented in series with the single mode plant dynamics whereas all other loop components are modeled as being perfect. Note that the rigid-body inertia J has been absorbed by the two PD gains.

For a rigid plant, or alternatively for $\alpha_k = 1$, the control gains K_p, K_d, needed to assure a specified closed-loop bandwidth ω_B, are given by

$$K_p = (\sqrt{4\zeta_B^4 + 4\zeta_B^2 + 2} - 2\zeta_B^2 - 1)\omega_B^2 \tag{9a}$$

$$K_d = 2\zeta_B\sqrt{K_p} \tag{9b}$$

where ζ_B is the desired damping (usually $\zeta_B = 1/\sqrt{2}$) of the closed-loop poles. To clarify matters, the closed-loop bandwidth ω_B is the frequency below which the magnitude of the closed-loop response remains within 3 dB. Selection of loop bandwidth to meet pointing performance requirements (i.e., rise time, overshoot, long-term pointing stability or jitter, etc.) on the basis of the rigid-plant assumption is straightforward. The key question of interest is: what happens to stability and performance when flexibility is introduced?

This study will only address the issue of stability. The fourth-order characteristic equation governing closed-loop stability is

$$s^4 + (K_d\alpha_k + 2\zeta\omega_k)s^3 + (2\zeta\omega_k K_d + \alpha_k K_p + \omega_k^2)s^2 + (2\zeta\omega_k K_p + K_d\omega_k^2)s + (K_p\omega_k^2) = 0 \tag{10}$$

The Routh criterion is employed to obtain the three nontrivial stability conditions

$$K_d\alpha_k + 2\zeta\omega_k > 0 \tag{11a}$$

$$(K_pK_d)\alpha_k^2 + \omega_k(2\zeta K_p + 2\zeta K_d^2 + K_d\omega_k)\alpha_k + \omega_k(4\zeta^2\omega_k K_d + 2\zeta\omega_k^2 - 2\zeta K_p - K_d\omega_k) > 0 \tag{11b}$$

and

$$(2\zeta K_p^2 K_d)\alpha_k^2 + \omega_k(4\zeta^2 K_p^2 + 4\zeta^2 K_pK_d^2 + 2\zeta\omega_k K_d^3 + K_d^2\omega_k^2)\alpha_k + \omega_k(8\zeta^3\omega_k K_pK_d + 4\zeta^2\omega_k^2 K_d^2 - 4\zeta^2 K_p^2 + 2\zeta\omega_k^3 K_d - 4\zeta\omega_k K_pK_d - K_d^2\omega_k^2) > 0 \tag{11c}$$

With modal frequency ω_k, damping ζ, and loop bandwidth ω_B varying, the above conditions can be forced to zero and plotted in the ω_k, α_k plane revealing the region of stability parametrically. Note that the first condition [Eq. (11a)] is linear in α_k, whereas the second and third conditions [Eqs. (11b) and (11c)] are quadratic in α_k. This means that for each value of the parameters K_p, K_d, ζ, ω_k, five different values of α_k are possible. As ω_k is varied, the stability boundary can be obtained by checking the roots of Eq. (10) around each of the five branches and identifying the correct one. For the particular cases studied herein, the dominant condition governing stability was the first of the two roots of Eq. (11c).

In order to make meaningful observations with clarity, the modal participation coefficient α_k is plotted against modal frequency normalized with respect to bandwidth ω_k/ω_B. Figure 5 shows what happens to the stability boundary when modal damping takes on the values of 0.2%, 1%, and 5% of critical. On the basis of these results, the following observations are made.

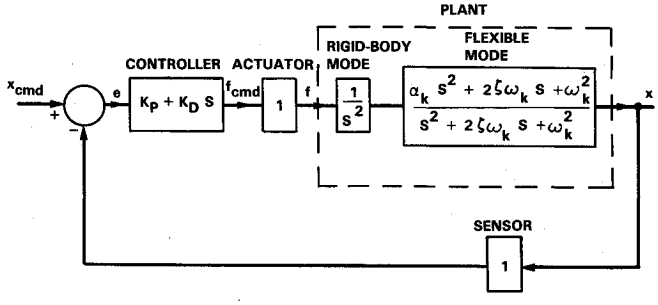

Fig. 4 Servo loop model with perfect sensor.

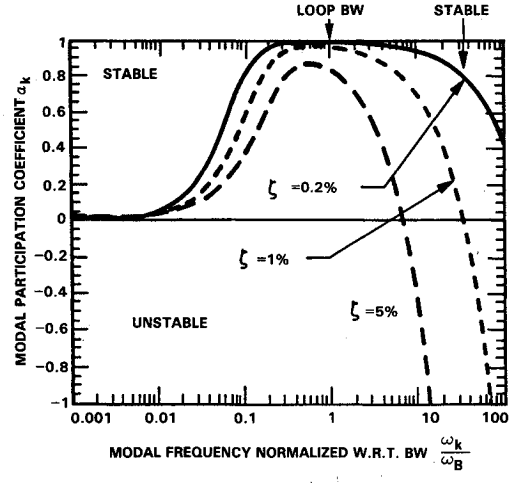

Fig. 5 Effect of damping on stability (perfect sensor).

1) An appendage mode at any frequency will not be driven unstable. This is evident since the stability boundary does not extend into the $\alpha_k > 1$ region.

2) An in-the-loop minimum phase mode can be easily destabilized if it occurs near the control bandwidth. The allowable margin is due to the damping of the structure. Although the dangerous area is 1 order of magnitude around the bandwith, a safe distance of 2 orders of magnitude lower or higher than the bandwidth is suggested by the result in Fig. 5 (assuming $\zeta = 0.2\%$).

3) An in-the-loop nonminimum phase mode located at a frequency less than 2 orders of magnitude from the loop bandwidth will be driven unstable (assuming $\zeta = 0.2\%$). Again, this is clearly evident from Fig. 5.

Obviously, a very high frequency mode will be gain-stabilized by the steep loop roll-off. The key observation here is that modes as high as 2 orders of magnitude away from the bandwidth can cause instability. This is contrary to the popular belief claiming that only modes within 1 order of magnitude away from the bandwidth can be troublesome. But as will be seen next, finite roll-off dynamics inserted in the feedback path significantly affect the above results.

Finite-Sensor Bandwidth

The previous analysis is now repeated for finite-sensor bandwidth. The loop block diagram of Fig. 6 shows the update in the dynamics of the feedback path. The second-order model chosen is commonly used as an attempt to capture the effects of sensor roll-off. Although this model has been referred to as a sensor model, it may just as easily represent a control filter designed to eliminate sensor noise or prevent aliasing in digital computer implementations. The actuator in the forward path is still assumed perfect, since modeling its linear finite-bandwidth dynamics unnecessarily complicates the loop model, while it is not expected to provide additional insight into the problem.

Assuming that the plant is rigid (i.e., $\alpha_k = 1$) and in view of the finite-sensor roll-off, a necessary and sufficient condition for stability is

$$2\zeta_s\omega_s K_d - 4\zeta_s^2 K_p - K_d^2 > 0 \qquad (12)$$

where ζ_s is the damping of the sensor poles (usually $\zeta_s = 1/\sqrt{2}$). This indicates that in the presence of finite-sensor bandwidth an attempt to raise the control gains beyond the limit of Eq. (12) will destabilize the rigid-body mode. Of course, now the exact relation between closed-loop bandwidth ω_B and the gains K_p, K_d is more complicated than it is shown in Eq. (9). Nevertheless, assuming that Eq. (12) is satisfied, the sixth-order characteristic equation governing closed-loop stability is

$$\begin{aligned} &s^6 + (2\zeta\omega_k + 2\zeta_s\omega_s)s^5 + (4\zeta\omega_k\zeta_s\omega_s + \omega_k^2 + \omega_s^2)s^4 \\ &\quad + (\alpha_k K_d\omega_s^2 + 2\zeta\omega_k\omega_s^2 + 2\zeta_s\omega_s\omega_k^2)s^3 \\ &\quad + (\alpha_k K_p\omega_s^2 + 2\zeta\omega_k\omega_s^2 K_d + \omega_k^2\omega_s^2)s^2 \\ &\quad + (2\zeta\omega_k\omega_s^2 K_p + K_d\omega_k^2\omega_s^2)s + (K_p\omega_k^2\omega_s^2) = 0 \end{aligned} \qquad (13)$$

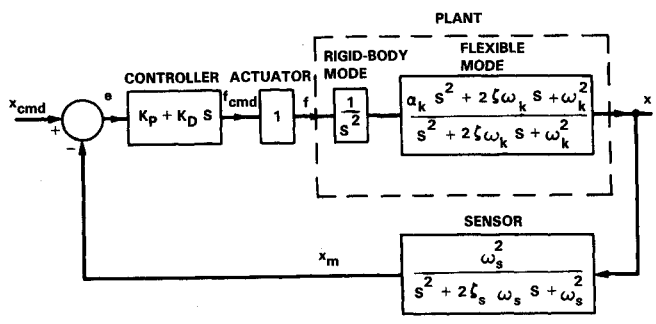

Fig. 6 Servo loop model with finite-sensor bandwidth.

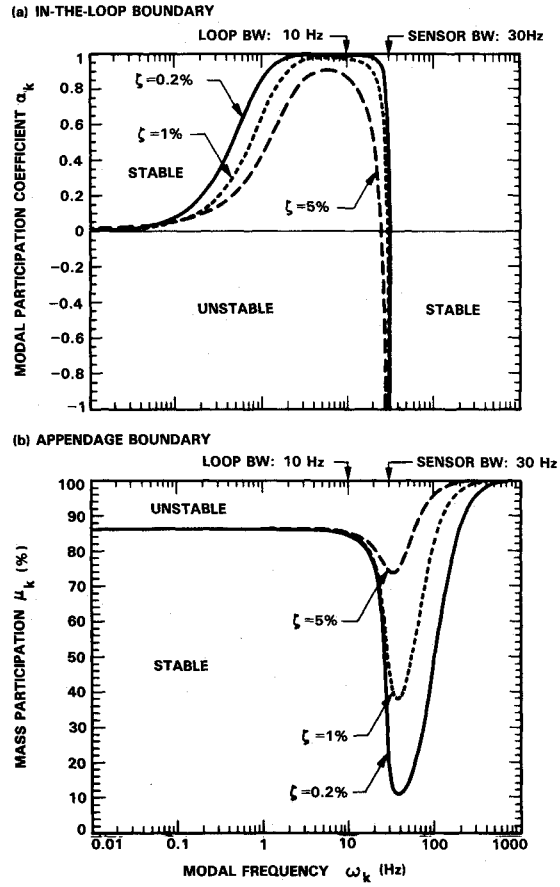

Fig. 7 Effect of damping on stability ($\omega_s/\omega_B = 3$).

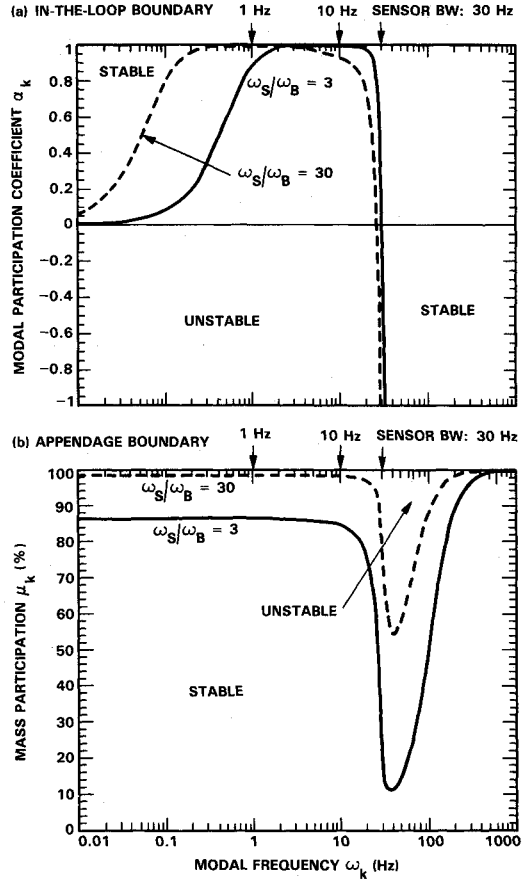

Fig. 8 Effect of loop bandwidth on stability ($\zeta = 0.2\%$).

The Routh criterion is again used to obtain four nontrivial stability conditions. However, this time the task of deriving close form expressions is extremely difficult. The symbolic manipulator program MACSYMA[17] was employed to perform all the algebraic operations needed to obtain the conditions, as well as to prepare the corresponding FORTRAN code used in the trade studies. Because of the length and complexity of the expressions, they will not be listed here, but relevant items of interest will be discussed. The stability conditions were put in the form of polynomials in the modal participation coefficient α_k, similar to those of Eq. (11). The first condition was linear, the second was quadratic, and the last two were cubic in α_k. Following a similar procedure as before, stability boundaries for in-the-loop modes were plotted in the ω_k,α_k plane, whereas for appendage modes the ω_k,μ_k plane was used. The additional parameters ζ_s,ω_s associated with the sensor model were set to 70.7% and 60π rad/s (30 Hz), respectively. This enabled trade studies with 3:1 and 30:1 sensor-to-loop bandwidths. The results are illustrated in Figs. 7 and 8.

Comparing these results with those obtained in the case of infinite-sensor bandwidth, one notes significant differences. The following observations are made.

1) An appendage mode can now be driven unstable. Instability is more likely to occur if the modal frequency is near or just outside the sensor bandwidth. As shown in Fig. 8b, this does not depend on the loop bandwidth, although the stability margin is increased considerably when control gains corresponding to a lower loop bandwidth are used.

2) An in-the-loop minimum phase mode near the loop bandwidth can be easily destabilized. However, this type of mode will not be driven unstable if its frequency is higher than the sensor bandwidth. This important result is clearly evident in Figs. 7a and 8a. Of course, if the sensor bandwidth is much higher than the control bandwidth (i.e., 2 orders of magnitude or higher) the perfect sensor result of Fig. 5 is valid.

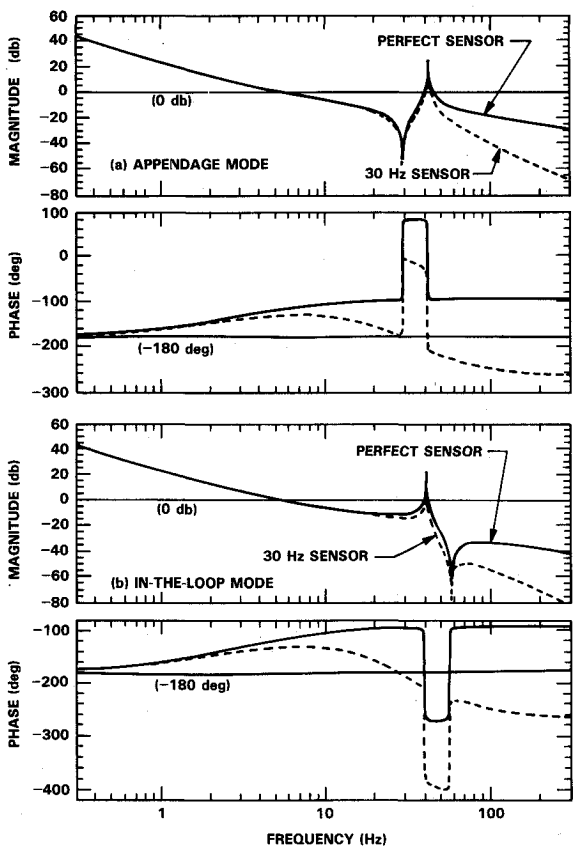

Fig. 9 Frequency response interpretation of the effect of finite-sensor bandwidth on stability.

3) An in-the-loop nonminimum phase mode will be unstable provided that its frequency is lower than the sensor bandwidth, while stability is expected if it is higher.

These observations strongly suggest that a second-order low-pass element placed in the feedback path may produce a stable control-structure interaction with in-the-loop-type flexibility. On the other hand, this action may cause an unstable interaction with appendage flexibility, especially in the region of the low-pass break frequency. Qualitatively, the results described above could also be observed by plotting the root locus of Eq. (13). However, the benefit of this analysis is that quantitative information is additionally extracted from a stability boundary drawn in the frequency/mode-shape plane.

Example

In order to better understand the results obtained from stability analysis, a specific single mode example addressing appendage and in-the-loop modes is analyzed. Consider the servo loop model of Fig. 6 with the following parameters: 1) modal frequency $\omega_k = 80\pi$ rad/s (40 Hz); 2) modal damping $\zeta = 0.2\%$; 3) appendage coefficient $\alpha_k = 2$; 4) in-the-loop coefficient $\alpha_k = 0.5$; 5) loop bandwidth $\omega_B = 20\pi$ rad/s (10 Hz); and 6) sensor bandwidth $\omega_s = 60\pi$ rad/s (30 Hz).

Frequency response plots of the above example are shown in Fig. 9. To illustrate the effect of finite-sensor bandwidth, these are compared with frequency response plots of an equivalent system employing a perfect sensor. With the modal frequency, loop bandwidth, and sensor bandwidth so close in frequency, gain stabilization due to the rigid-body and sensor roll-off does not occur. The key effect here is the amount of phase taken away by the sensor. For the appendage mode (Fig. 9a), a perfect sensor shows a stable mode, but the 30 Hz sensor shifts the phase plot down and under the −180 deg line yielding negative phase margin at the third gain crossover, and thus destabilizes the mode. On the other hand, for the in-the-loop mode (Fig. 9b), a perfect sensor shows instability, whereas the finite-bandwidth sensor shifts the phase plot down and away from the −180 deg line in the region of the resonance, and thus stabilizes the mode. Clearly, the finite-bandwidth sensor (second-order dynamics) has a destabilizing effect on the appendage mode, whereas it has a stabilizing effect on the

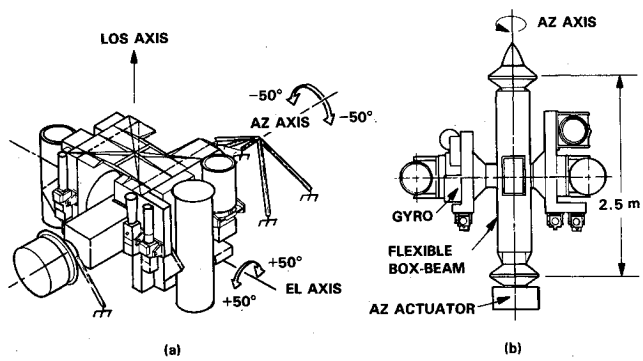

Fig. 10 Pathfinder gimbal pointer illustrating the separation of actuator and gyro.

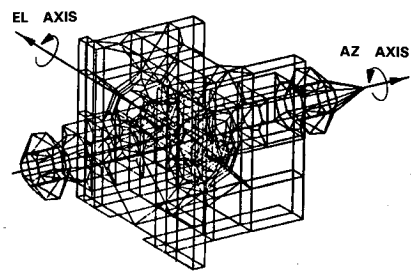

Fig. 11 Pathfinder NASTRAN model.

in-the-loop mode. This provides a frequency response interpretation as well as a confirmation of the results obtained from stability analysis.

Pathfinder Gimbal Pointer

Attention will now be shifted to the study of a more realistic multimode structural system. The remainder of the paper will address the gimbal structure shown in Fig. 10. This is the Pathfinder gimbal (and shall be referred to as such) designed at JPL for a proposed mission. It is a two-axis, nearly symmetric, center-of-mass mounted pointer to be used in the Space Shuttle Orbiter for precision pointing and tracking applications. A tracking camera measures the pointing error, and a corresponding control law issues inertial rate commands to a high bandwidth gyro loop.[18] The gyro loop is the heart of the control system, and its main function is to reject disturbances arising from system hardware (i.e., bearings, motors, etc.) and base-body motion. The loop bandwidth necessary for adequate disturbance rejection, assuming a rigid gimbal, was estimated at 10 Hz, while the associated control law architecture was that of a PI on rate. The azimuth (AZ) and elevation (EL) axes were independently servoed. The gyro used in the design was a DRIRU-II unit[19] whose bandwidth was extended to 30 Hz. Reactionless two-motor actuators were used to provide the control torques while leaving the flexible base body undisturbed.[20] These employed current feedback and their bandwidth was an order of magnitude higher than that of the gyro.

The above description fits the servo loop model of Fig. 6 quite well. The main difference is the plant model. A second look at Fig. 10b reveals that the AZ actuator is separated from the gyro by the flexible box-beam gimbal. This indicates that significant in-the-loop flexibility is to be expected in the AZ servo loop. A NASTRAN finite-element model was erected (Fig. 11) for the purposes of addressing the severity of the control-structure interaction problem. In view of the 10 Hz loop bandwidth, all modes in the 0–200 Hz frequency range

Table 1 Pathfinder structural data

Elastic mode	Structural frequency, Hz	Single mode model parameters	
		α_k	μ_k
1	25.3	0.999	
2	29.1	1.000	0.012
3	29.9	1.004	0.490
4	36.7	1.000	0.004
5	61.8	2.030	50.747
6	68.5	1.043	4.156
7	78.6	1.005	0.516
8	80.8	1.001	0.187
9	90.9	1.271	21.361
10	92.7	1.035	3.417
11	94.9	0.999	—
12	106.9	0.999	—
13	110.0	1.147	12.859
14	113.9	0.728	—
15	122.4	0.992	—
16	131.9	0.997	—
17	138.6	1.554	35.683
18	143.6	1.114	10.231
19	150.2	0.260	—
20	155.4	0.969	—
21	155.5	0.979	—
22	157.7	0.515	—
23	162.8	1.061	5.824
24	163.1	0.903	—
25	166.6	0.798	—
26	169.0	0.927	—
27	175.6	0.759	—
28	189.2	2.341	57.283

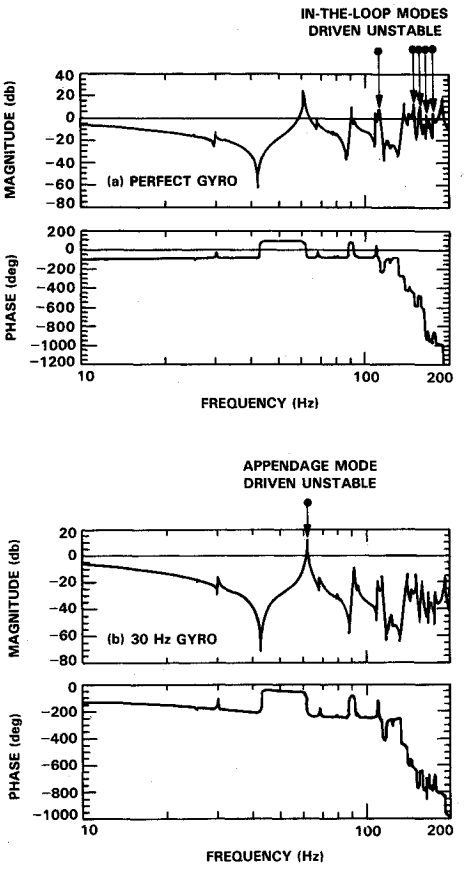

Fig. 12 Effect of gyro bandwidth on pathfinder servo loop stability.

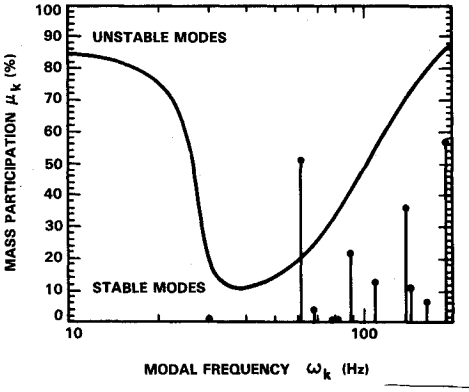

Fig. 13 Single mode treatment of the 28-mode model correctly predicting the 62 Hz unstable appendage mode.

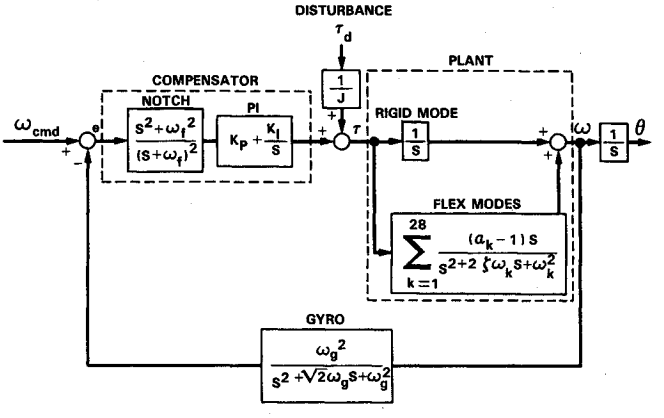

Fig. 14 Servo loop block diagram.

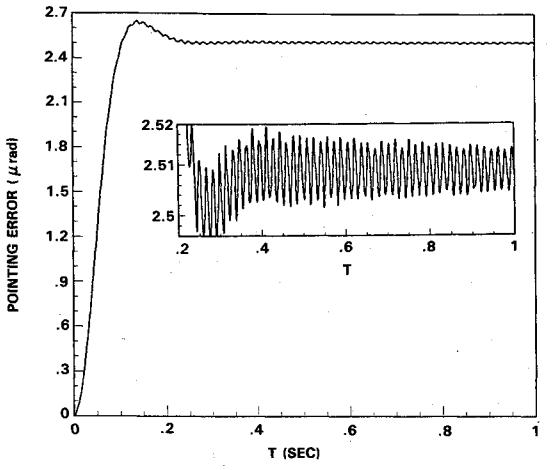

Fig. 15 Disturbance rejection of a 1 N-m constant bias.

(28 of them were elastic) were extracted and used to represent the plant model in accordance with Eq. (1). Pertinent structural data associated with the 28 elastic modes are listed in Table 1. Inspection of the modal participation coefficients indicates that exactly half of these modes are of the appendage type whereas the other half are of the in-the-loop minimum phase type. Nonminimum phase modes occur at much higher frequencies, and efforts to model them would unnecessarily complicate the analysis.

As in the case of the single mode example, frequency response analysis of the high-order servo loop model was performed and the results are shown in Fig. 12. First, with the gyro assumed perfect, five high frequency in-the-loop modes were driven unstable (Fig. 12a). It should be pointed out that the unstable modes are about 15–20 times higher than the loop bandwidth. Also note that the strong appendage mode at 62 Hz is a stable one. Second, with the gyro properly modeled as a second-order 30 Hz low-pass, all in-the-loop modes were gain-stabilized, while the 62 Hz appendage mode was now driven unstable (Fig. 12b). Superimposing the mass participation μ_k associated with the appendage modes over the stability boundary of Fig. 8b, the 62 Hz mode is shown unstable (Fig. 13). Therefore, in addition to providing insight into the control-structure interaction problem, single mode analysis correctly predicts the stability behavior of the Pathfinder multimode finite-element model.

The AZ servo loop block diagram of the Pathfinder gimbal pointer is shown in Fig. 14. A simple second-order notch filter[9] centered at the frequency of the unstable appendage mode ($\omega_f = 61.8$ Hz) was used to stabilize the system. The design provides 10 Hz closed-loop bandwidth ($K_p = 32.5$, $K_I = 527$) in the presence of the 30 Hz DRIRU-II gyro and an AZ axis inertia of 756 Kg-m^2. Furthermore, the phase and gain margins are 40 deg and 13 dB, respectively (both associated with the rigid-body mode), and all flexible modes are gain-stabilized. The disturbance rejection characteristics of the loop are clearly illustrated in Fig. 15. A 1 *N-m* constant bias disturbance acting at the actuator location produces a static error of 2.5 *microradians* ($1/K_1 J$) and a dynamic error less than 20 *nanoradians* (ringing of the "notched" mode).

Conclusion

Stability analysis of a linear sixth-order servo loop model was performed, shedding considerable insight into the control-structure interaction problem. Flexible modes were categorized into 1) appendage, 2) in-the-loop minimum phase, and 3) in-the-loop nonminimum phase via a finite-element derived single mode plant model. It was shown that a second-order low-pass element in the feedback path has a stabilizing effect on in-the-loop-type modes occurring at frequencies higher than its bandwidth at the expense of destabilizing appendage-type modes occurring near its bandwidth. In-the-loop modes strongly depend on actuator-sensor placement and are extremely dangerous at frequencies near the loop bandwidth. For precision pointing servo loops employing low-bandwidth inertial sensors such as the DRIRU-II gyro, stability problems may arise from appendage modes occurring at frequencies near the sensor bandwidth. Frequency response analysis of single and multimode examples demonstrated that second-order low-pass dynamics in the loop may stabilize/destabilize flexible modes by both phase lag and gain roll-off. In the case of the Pathfinder gimbal pointer, classical gain stabilization by means of a second-order notch filter was used to produce a high performance compensator.

Acknowledgment

The research described in this paper was carried out at the Jet Propulsion Laboratory, California Institute of Technology, under contract with NASA.

References

[1]Gevarter, W. B., "Basic Relations for Control of Flexible Vehicles," *AIAA Journal*, Vol. 8, April 1970, pp. 666–672.

[2]Martin, G. D., "On the Control of Flexible Mechanical Systems," Ph.D. Thesis, Dept. of Aeronautics and Astronautics, Stanford Univ., Stanford, CA, SUDAAR 511, May 1978.

[3]Wie, B. and Plescia, C. T., "Attitude Stabilization of a Flexible Spacecraft During Stationkeeping Maneuvers," *Journal of Guidance, Control, and Dynamics*, Vol. 7, July–Aug. 1984, pp. 430–436.

[4]Goh, C. J. and Caughey, T. K., "On the Stability Problem Caused by Finite Actuator Dynamics in the Collocated Control of Large Space Structures," *International Journal of Control*, Vol. 41, No. 3, 1985, pp. 787–802.

[5]Kopf, E. H., Brown, T. K., and Marsh, E. L., "Flexible Stator Control on the Galileo Spacecraft," AAS Paper 79-161, June 1979.

[6]Yocum, J. F. and Slafer, L. I., "Control System Design in the Presence of Severe Structural Dynamics Interactions," *Journal of Guidance, Control, and Dynamics*, Vol. 1, March–April 1978, pp. 109–116.

[7]Cannon, R. H. and Rosenthal, D. E., "Experiments in Control of Flexible Structures with Noncollocated Sensors and Actuators," *Journal of Guidance, Control, and Dynamics*, Vol. 7, Sept–Oct. 1984, pp. 564–553.

[8]Bell, C. E. and Lehman, D. E., "Mariner Mark II: Spacecraft Control for the 1990's and Beyond," AAS Paper 86-285, Oct. 1986.

[9]Wie, B. and Byun, K., "A New Concept of Generalized Structural Filtering for Active Vibration Control Synthesis," AIAA Paper 87-2456, Aug. 1987.

[10]Wie, B., "On the Modeling and Control of Flexible Space Structures," Ph.D. Thesis, Dept. of Aeronautics and Astronautics, Stanford Univ., Stanford, CA, SUDAAR 525, June 1981.

[11]Balas, M. J., "Feedback Control of Flexible Systems," *IEEE Transactions on Automatic Control*, Vol. AC-23, No. 4, Aug. 1978, pp. 673–679.

[12]Likins, P. W., "Dynamics and Control of Flexible Space Vehicles," TR 32-1329, Jet Propulsion Lab., Rev. 1, 1970.

[13]Porcelli, G., "Attitude Control of Flexible Space Vehicles," *AIAA Journal*, Vol. 10, June 1972, pp. 807–812.

[14]Edmunds, R. S., "Robust Control System Design Techniques for Large Flexible Space Structures Having Non-Collocated Sensors and Actuators," Ph.D. Thesis, Univ. of California, Los Angeles, 1982.

[15]Laskin, R. A. and Sirlin, S. W., "Future Payload Isolation and Pointing System Technology," *Journal of Guidance, Control, and Dynamics*, Vol. 9, July–Aug. 1986, pp. 469–477.

[16]Bamford, R. M., Wada, B. K., and Gayman, W. H., "Equivalent Spring-Mass System for Normal Modes," TM 33-380, Jet Propulsion Lab., Pasadena, CA, Feb. 1971.

[17]Bogen, R., *MACSYMA Reference Manual*, MATHLAB Group, Lab. for Computer Science, Massachusetts Inst. of Technology, Cambridge, MA, Version 9, Dec. 1977.

[18]Sirlin, S. W. and Bell, C. E., "Soft Mounted Momentum Compensated Pointing System for the Space Shuttle Orbiter," SPIE Paper 641-17, March–April 1986.

[19]*NASA Standard High Performance Inertial Reference Unit DRIRU-II*, Users Guide and Industry Briefing, Teledyne Systems Co., Cauoga Park, CA, Sept. 1983.

[20]Laskin, R. A., Kopf, E. H., Sirlin, S. W., Spanos, J. T., and Wiktor, P. J., "Reactionless Gimbal Actuation for Precise Pointing of Large Payloads," AAS Paper 87-512, Aug. 1987.